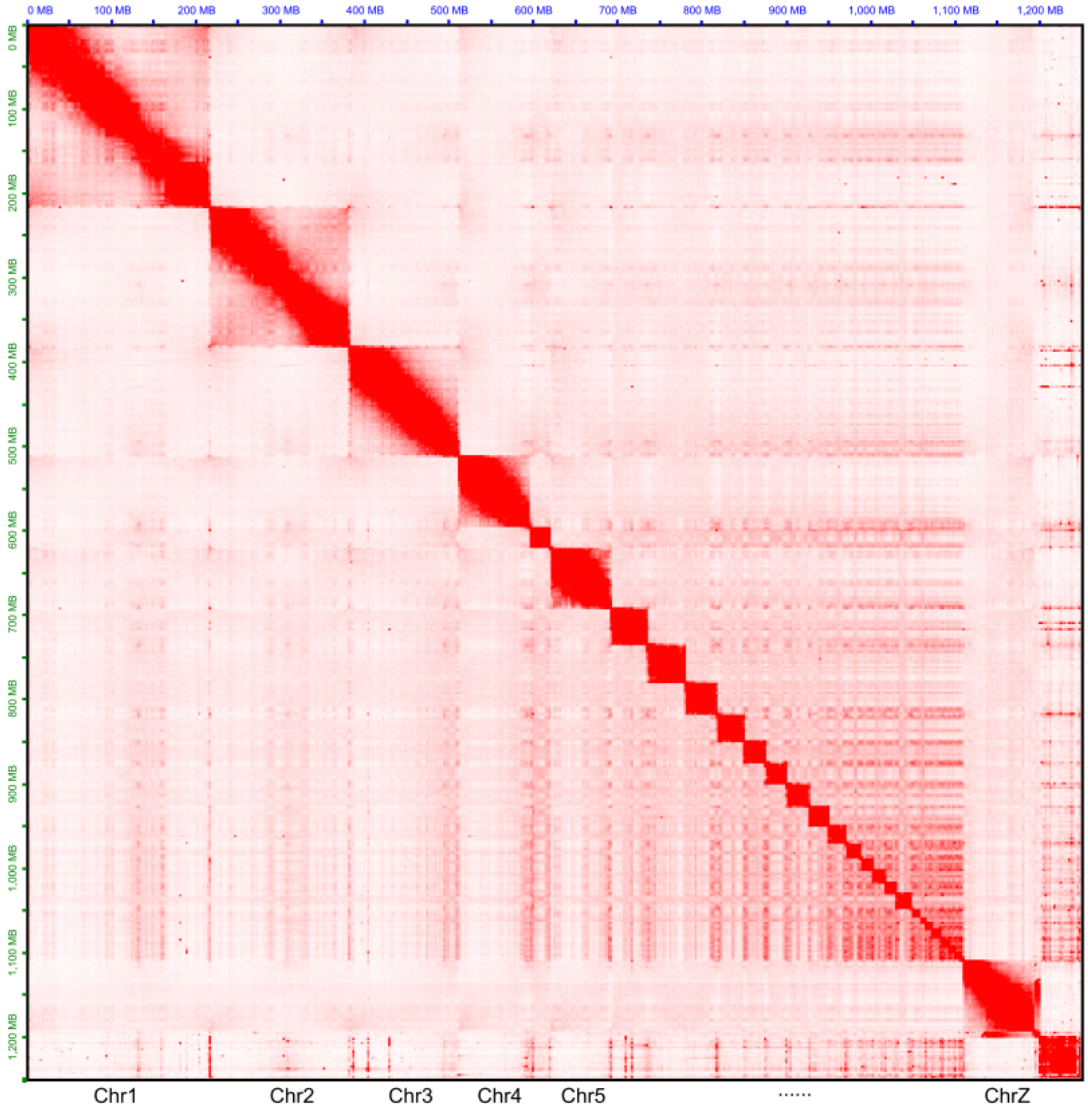

Supplemental Fig. S1. Chromosome-level assembly of droZJU1.0. The assembly was generated by combining PacBio long reads, 10x linked reads, Dovetail Chicago data, and Hi-C reads. The Hi-C map shows genome-wide all-by-all interactions visualized in Juicer tools, revealing little off diagonal interactions with other scaffolds in this curated assembly. The smaller autosomes and W are not labelled due to space constraints in the figure.

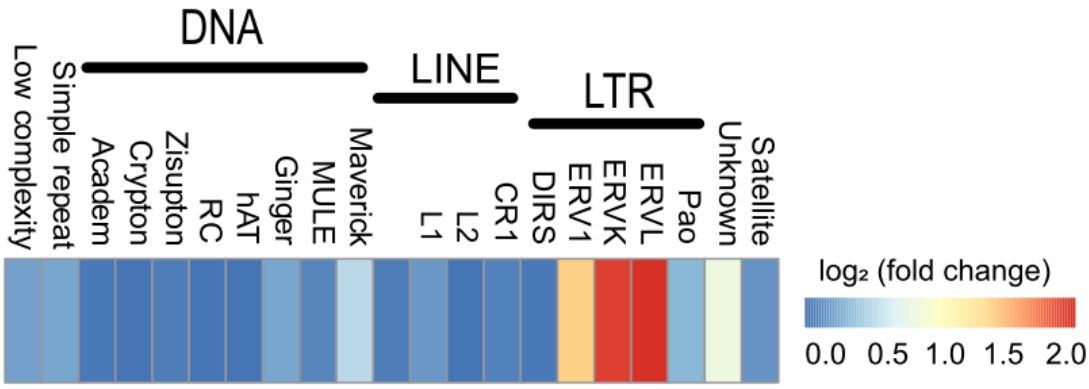

Supplemental Fig. S2. The fold change of all repeat families between droZJU1.0 and droNov1 assemblies. The PacBio reads based droZJU1.0 has generated increased LTR repeats compared to Illumina reads based droNov1.

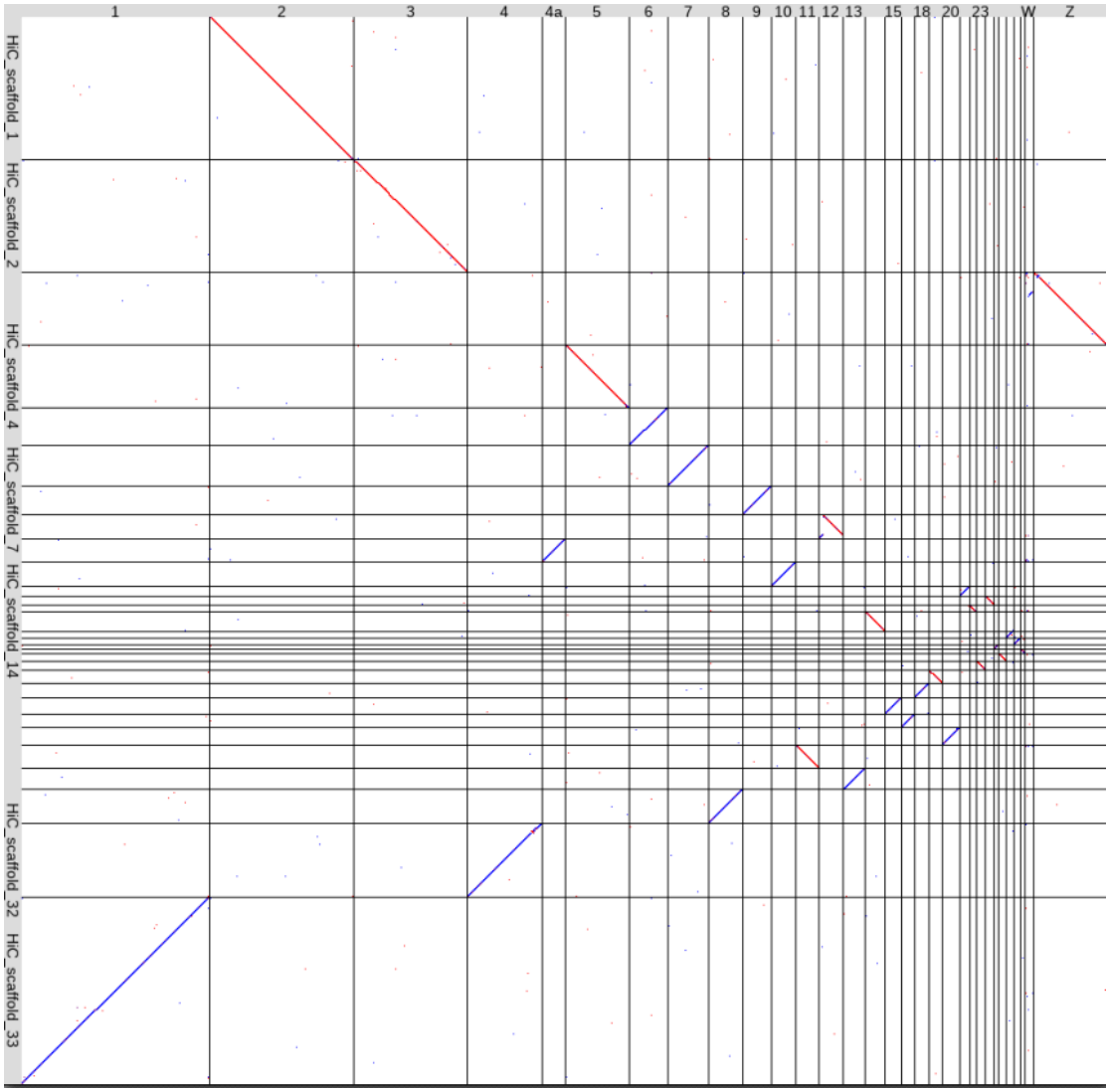

Supplemental Fig. S3. Genome comparison of droZJU1.0 and assembly from DNA zoo. Dot plot alignment of the genomes from this study (droZJU1.0) and DAN Zoo (DNAzoo) is shown. The x-axis represents droZJU1.0, and y-axis represents the assembly from DNA zoo, which is a Hi-C reads assembled version based on Illumina assembly droNov1. The highly consistent synteny suggests the accuracy of droZJU1.0.

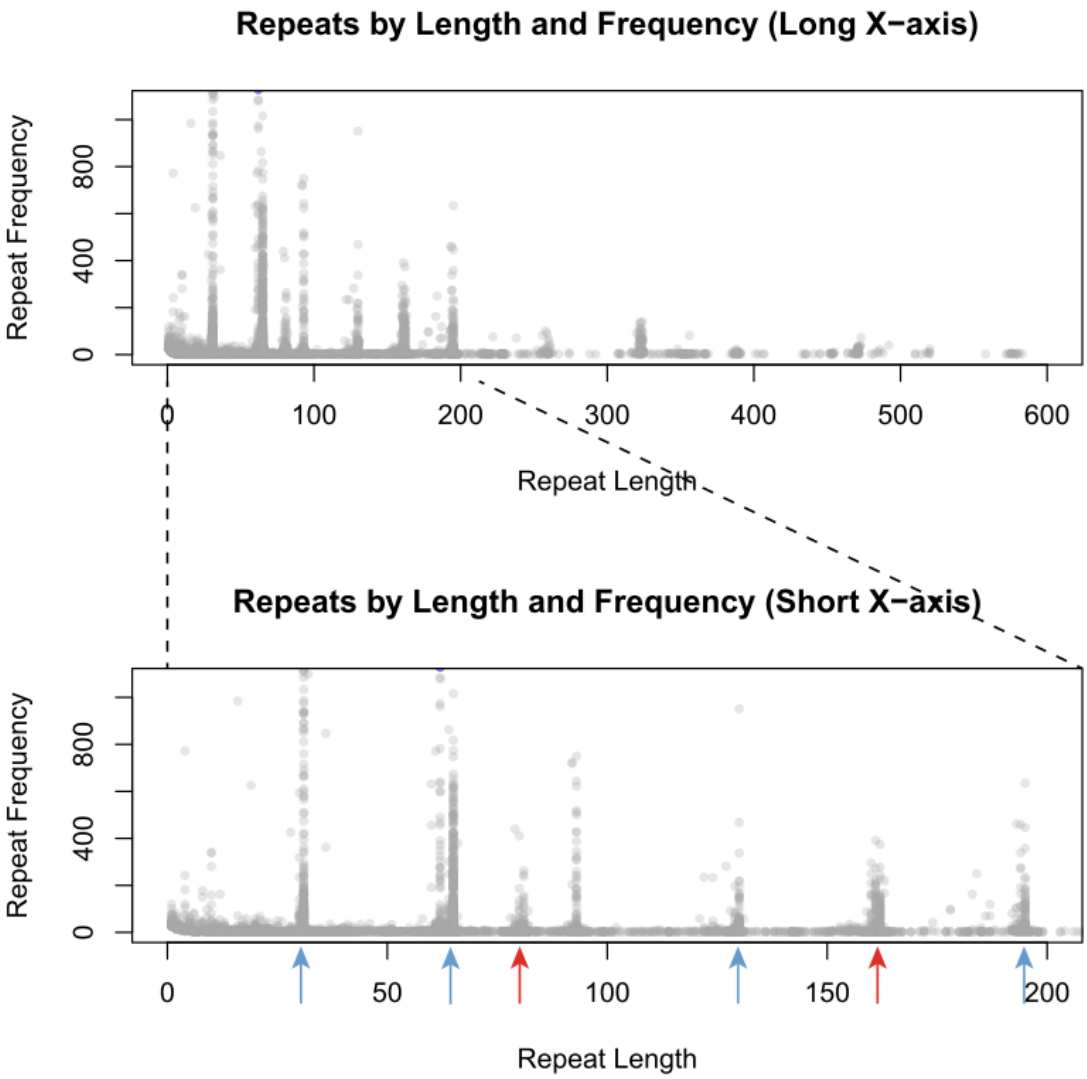

Supplemental Fig. S4. Distribution of tandem repeats on emu genome assembly. Tandem repeats with different sizes were detected by the software Tandem Repeats Finder. The putative centromere associated repeats are indicated by blue (65bp unit) and red arrows (81bp unit).

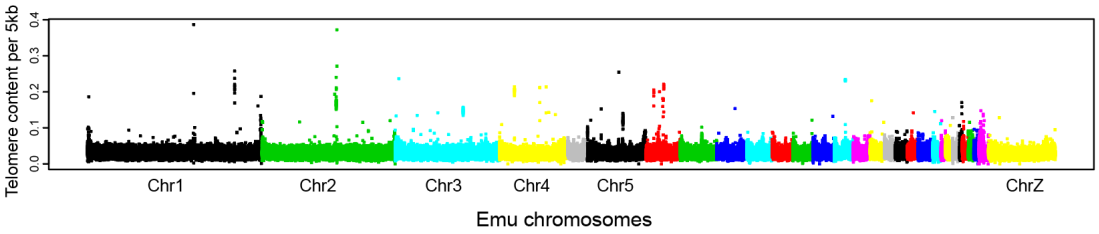

Supplemental Fig. S5. Manhattan plot of telomere density along each emu chromosome. The known vertebrate consensus sequence 'TTAGGG/CCCTAA' was used to search for the clusters of consensus sequences on both strands. Consensus sequence enriched genomic blocks in 5kb-window were then defined as the putative telomere regions.

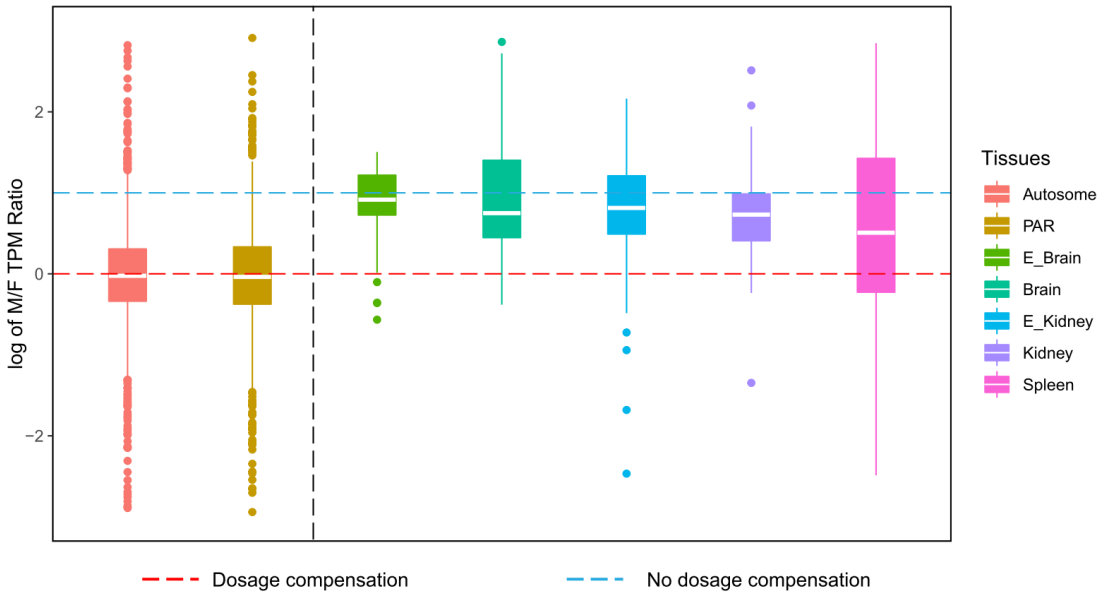

Supplemental Fig. S6. Incomplete dosage compensation on Z-linked S0 region. Shown are box plots of male-to-female (M/F) gene expression $\log_2$ ratio (transcripts per million: TPM) across different evolutionary strata and tissues is shown. We color-coded autosomes in red and PAR in yellow on left-part panel. Boxplots on right-part panel indicate gene expression $\log_2$ ratio in different tissues on Z-linked S0 region. The red horizontal and blue lines represent boundaries of complete dosage compensation and the absence, respectively.

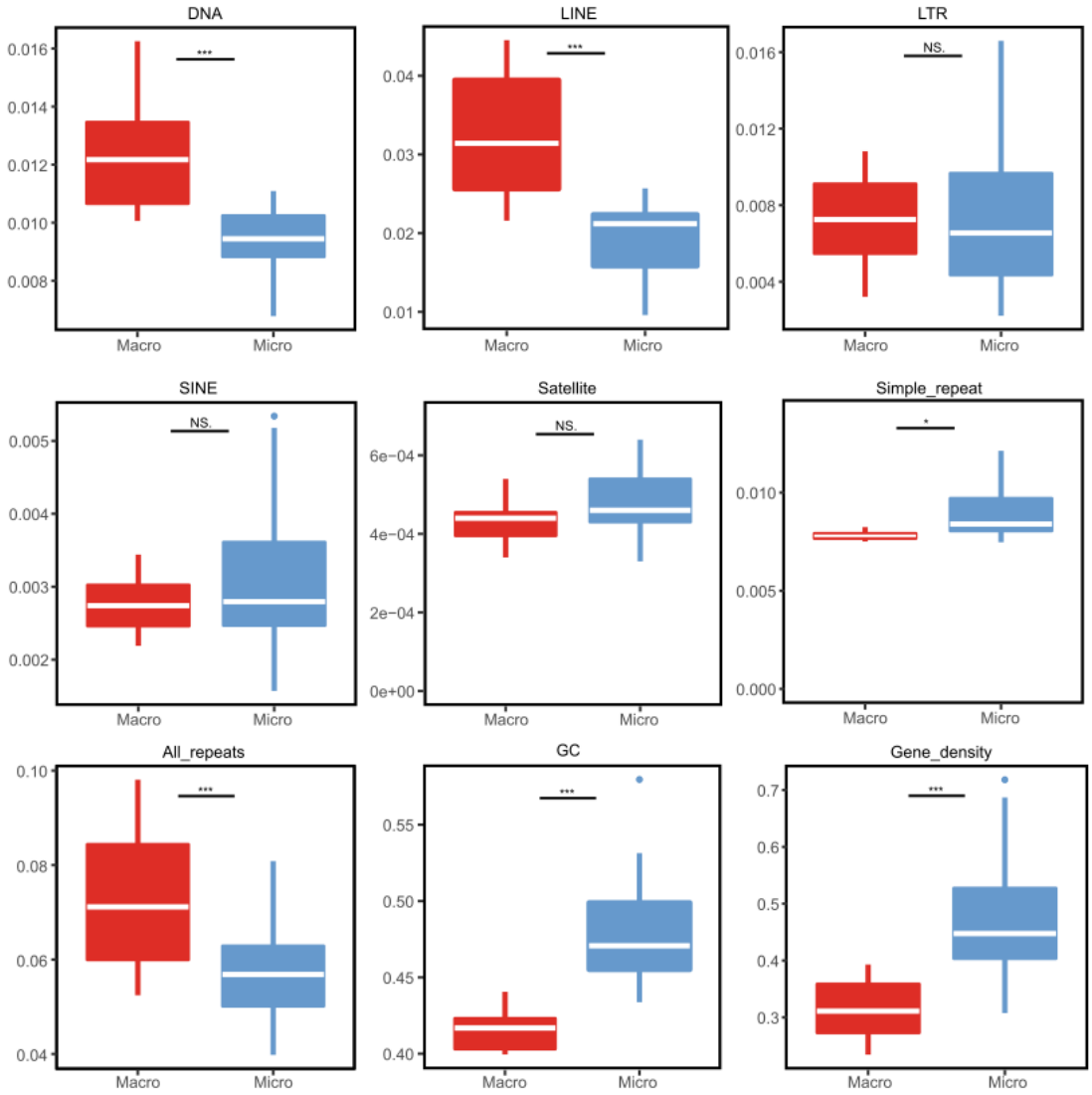

Supplemental Fig. S7 | Comparison of different genomic features between macro- and microchromosomes. The comparison with significant difference is shown with an asterisk on the top. *: $P < 0.05$; **: $P < 0.005$; ***: $P < 0.0005$.

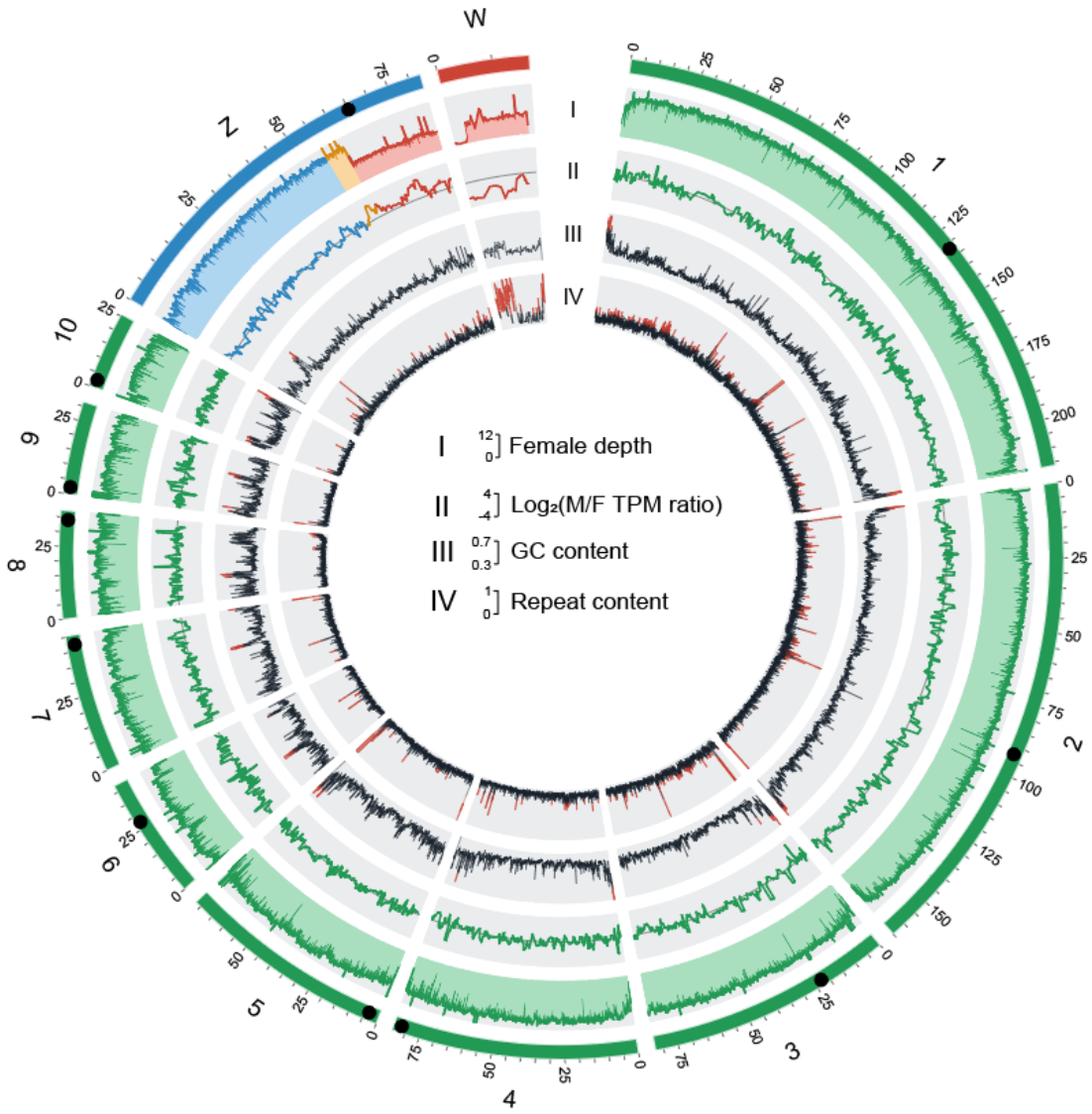

Supplemental Fig. S8. Genomic features of macrochromosomes. The PAR (blue) and autosomes (green) show a 2-fold higher female read coverage (the first ring) than the S1 (orange), S0 and ChrW (red). S0 shows a male-biased (the second ring) expression pattern. ChrW has a higher repeat content (the third ring) than the autosome and ChrZ. The plot was generated using circos-0.69-9.

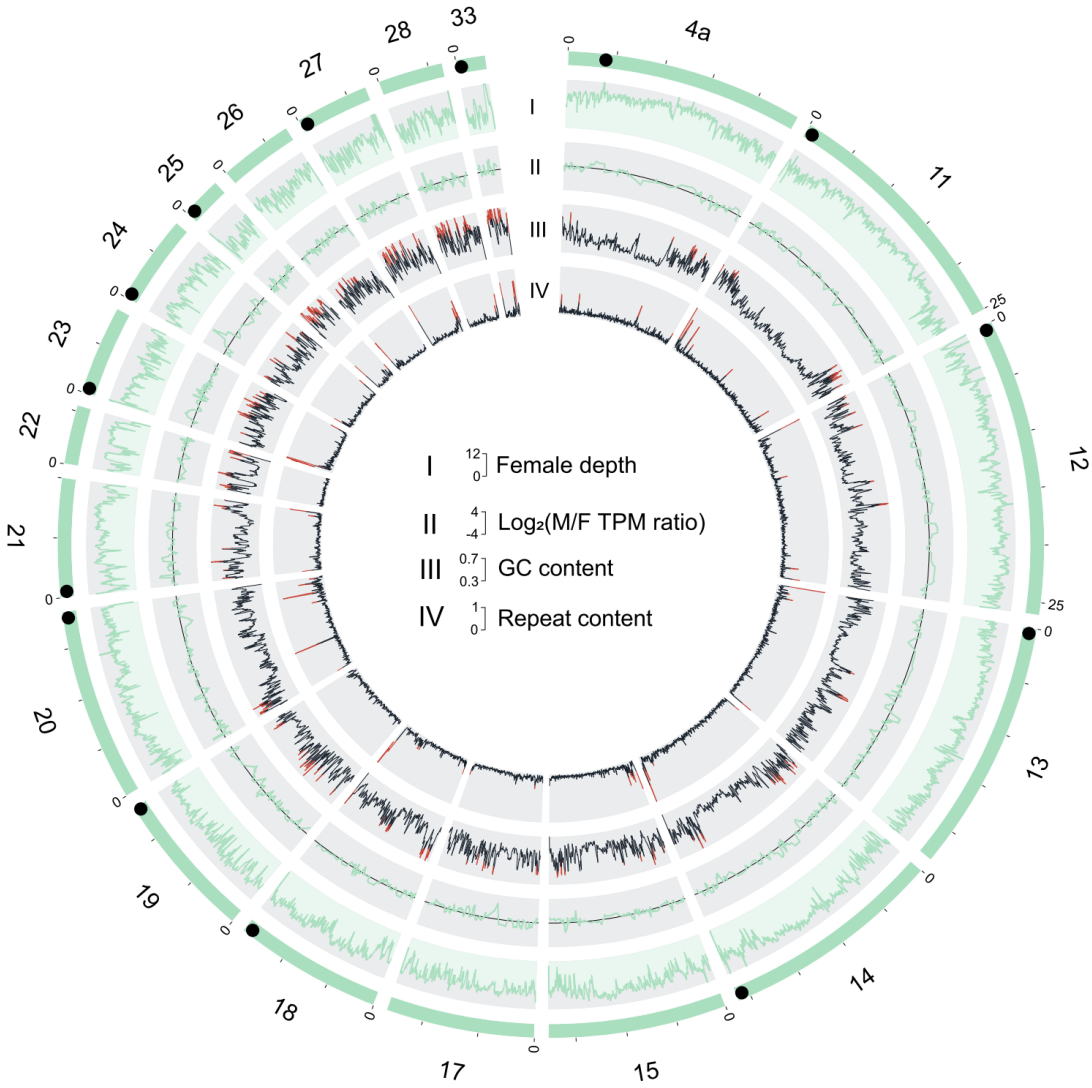

Supplemental Fig. S9. Genomic features of microchromosomes. The legend is similar as Supplemental Fig. S8.

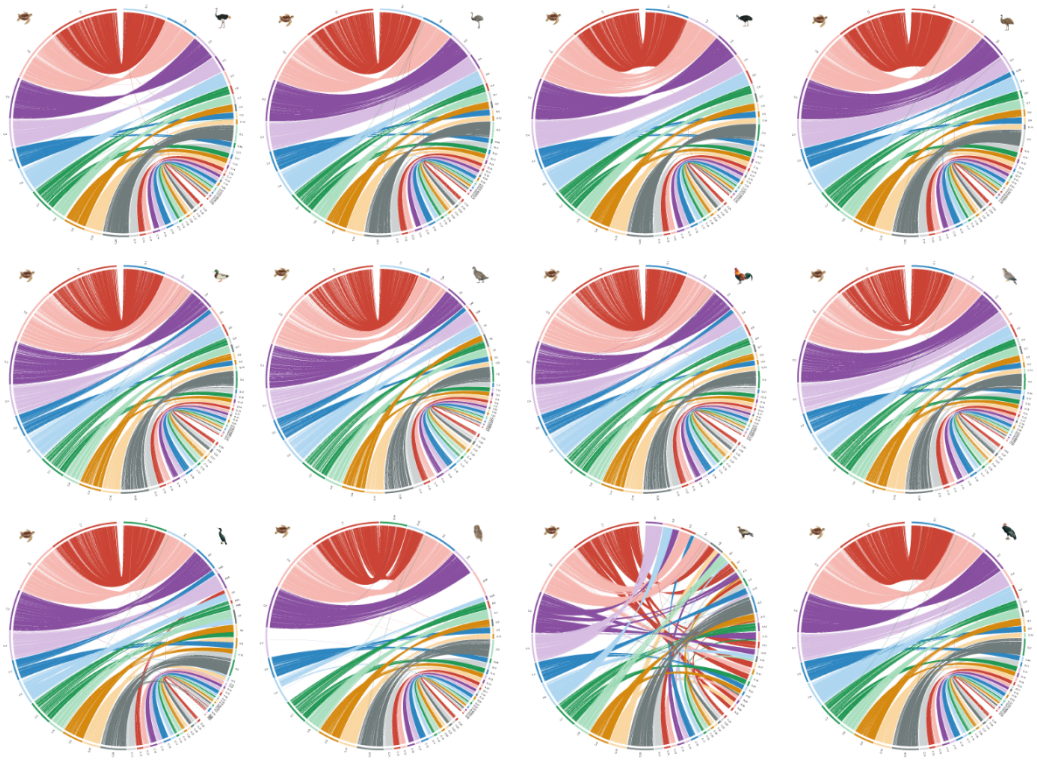

Supplemental Fig. S10. Synteny plots between birds and green sea turtle. From left to right, upper to lower, the bird names are common ostrich (*Struthio camelus*), greater rhea (*Rhea americana*), Southern cassowary (*Casuarius casuarius*), emu (*Dromaius novaehollandiae*), Peking duck (*Anas platyrhynchos*) (Unpublished), greater prairie chicken (*Tympanuchus cupido*), chicken (*Gallus gallus*), band-tailed pigeon (*Patagioenas fasciata*), double-crested cormorant (*Phalacrocorax auritus*), spotted owl (*Strix occidentalis*), golden eagle (*Aquila chrysaetos*), California condor (*Gymnogyps californianus*). The chromosomes are indicated by the first letter of the species name and chromosome number.

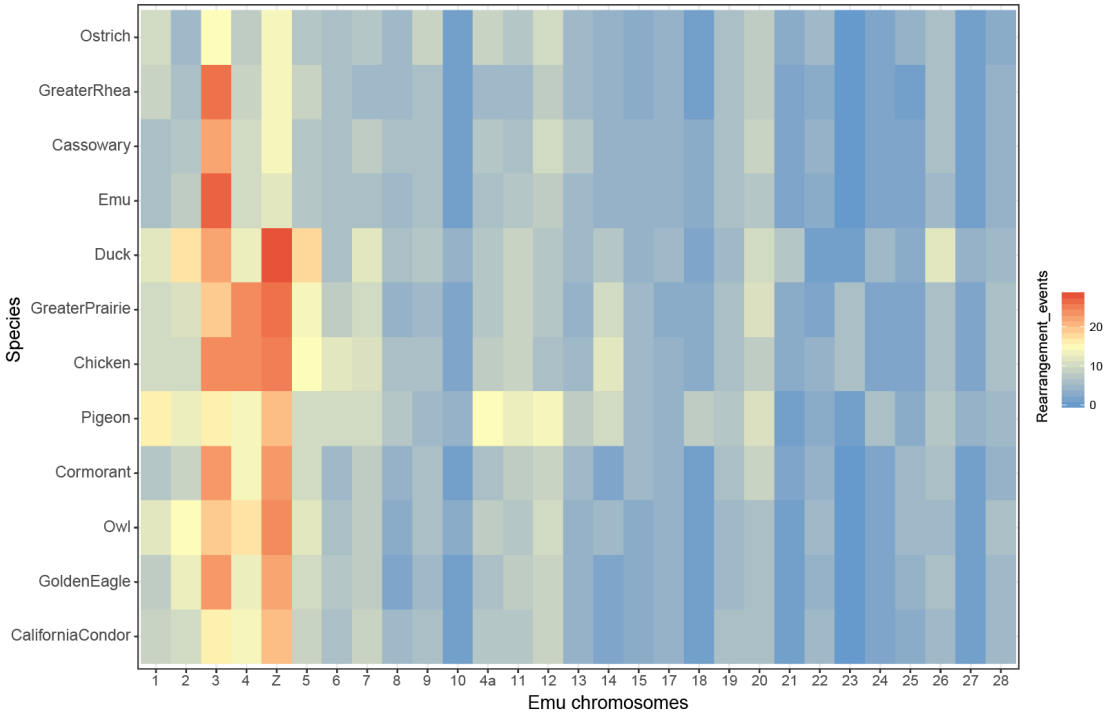

Supplemental Fig. S11. The numbers of intrachromosomal rearrangement number for all chromosomes of birds compared to the sea turtle are shown in the heatmap.

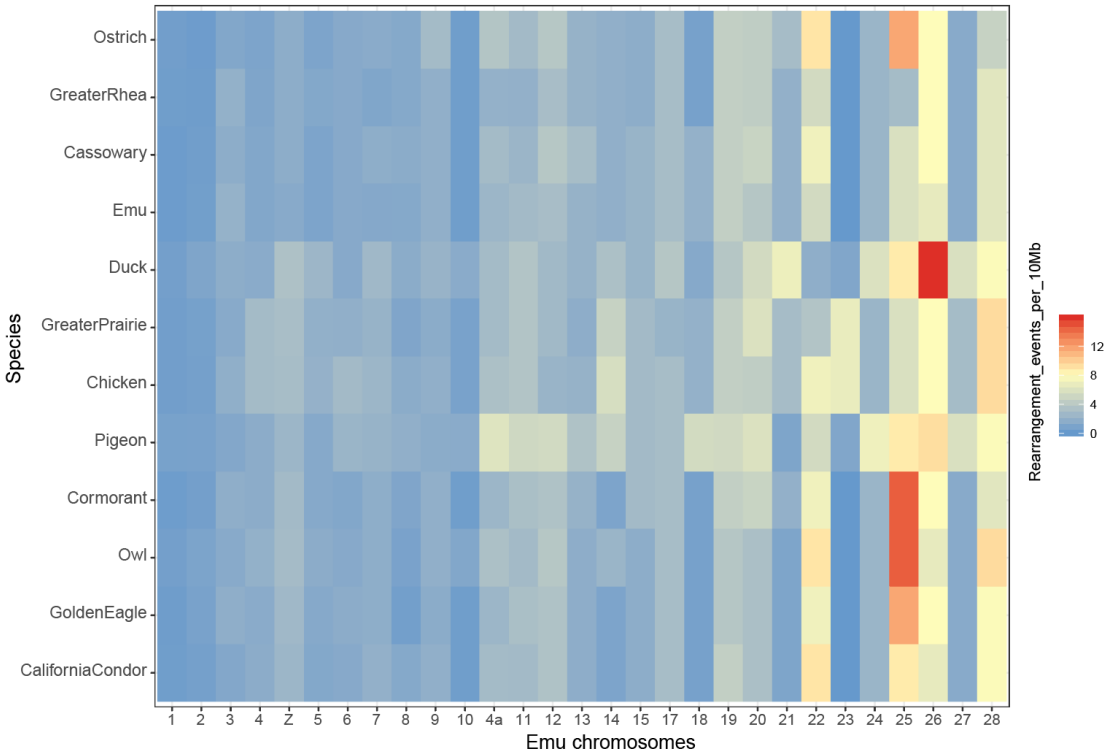

Supplemental Fig. S12. The numbers of intrachromosomal rearrangement number scaled with chromosome size for all chromosomes of birds compared to the sea turtle are shown in the heatmap.

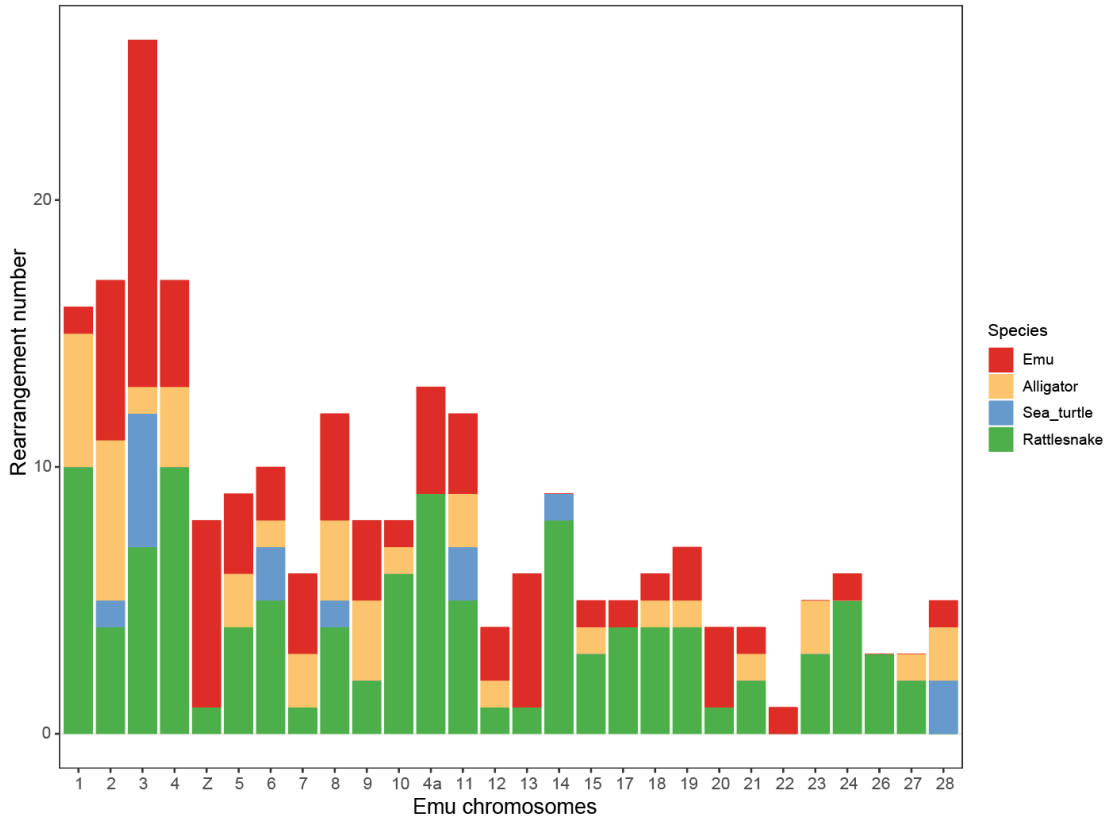

Supplemental Fig. S13. The intrachromosomal rearrangement number of different species since their divergence from the reptile ancestor. Each species' chromosomal genome was compared to the reconstructed reptile ancestral chromosomes to infer the number of rearrangements.

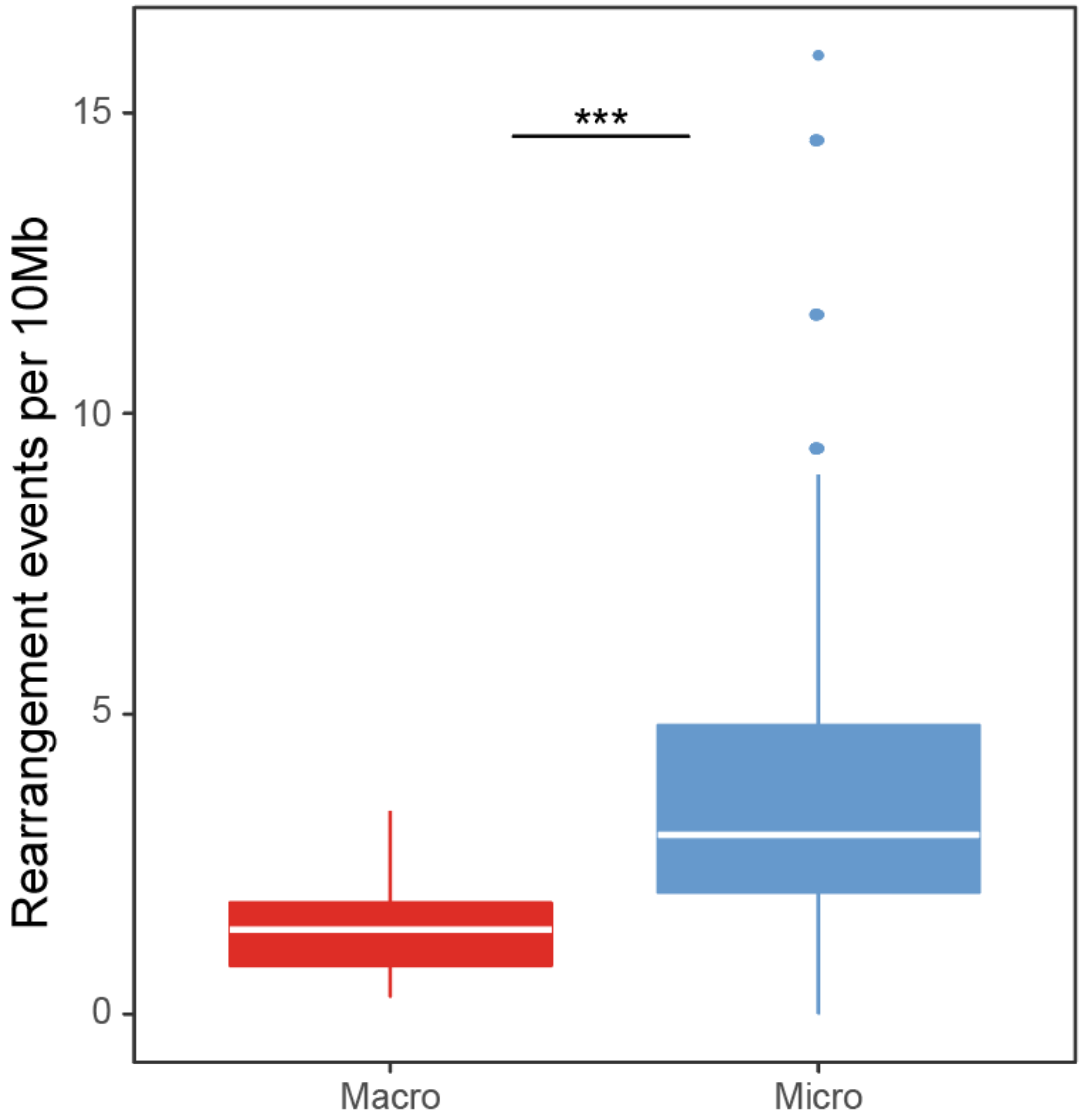

Supplemental Fig. S14. The RE number per 10Mb between macro- and microchromosomes after the removal of pigeon. ***: $P < 0.0005$.

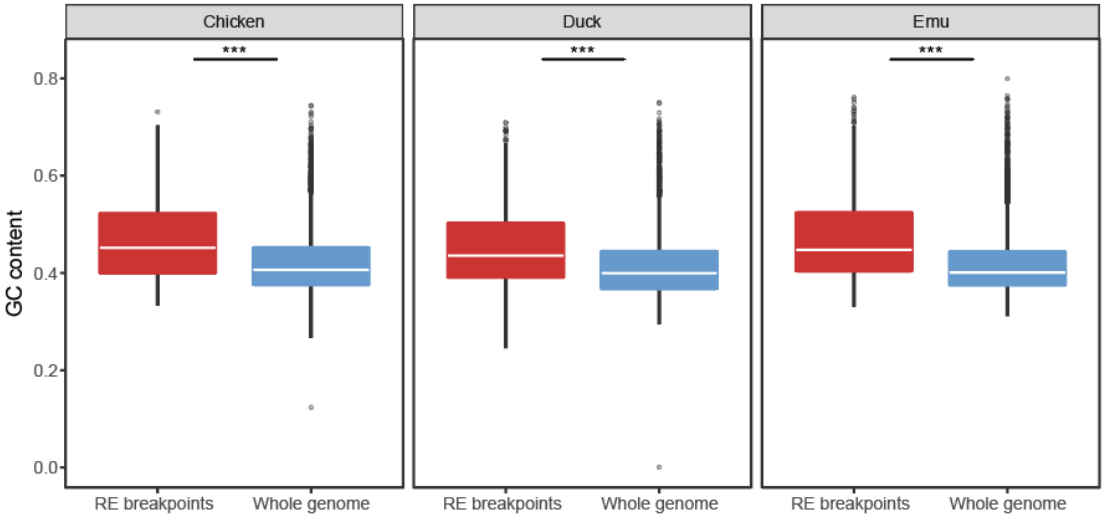

Supplemental Fig. S15. GC content comparison between RE breakpoints and the whole genome. Three PacBio reads based genome assemblies were used to calculate the GC contents. The rearrangement breakpoints show higher GC contents compared to the whole genome. ***: $P < 0.0005$.

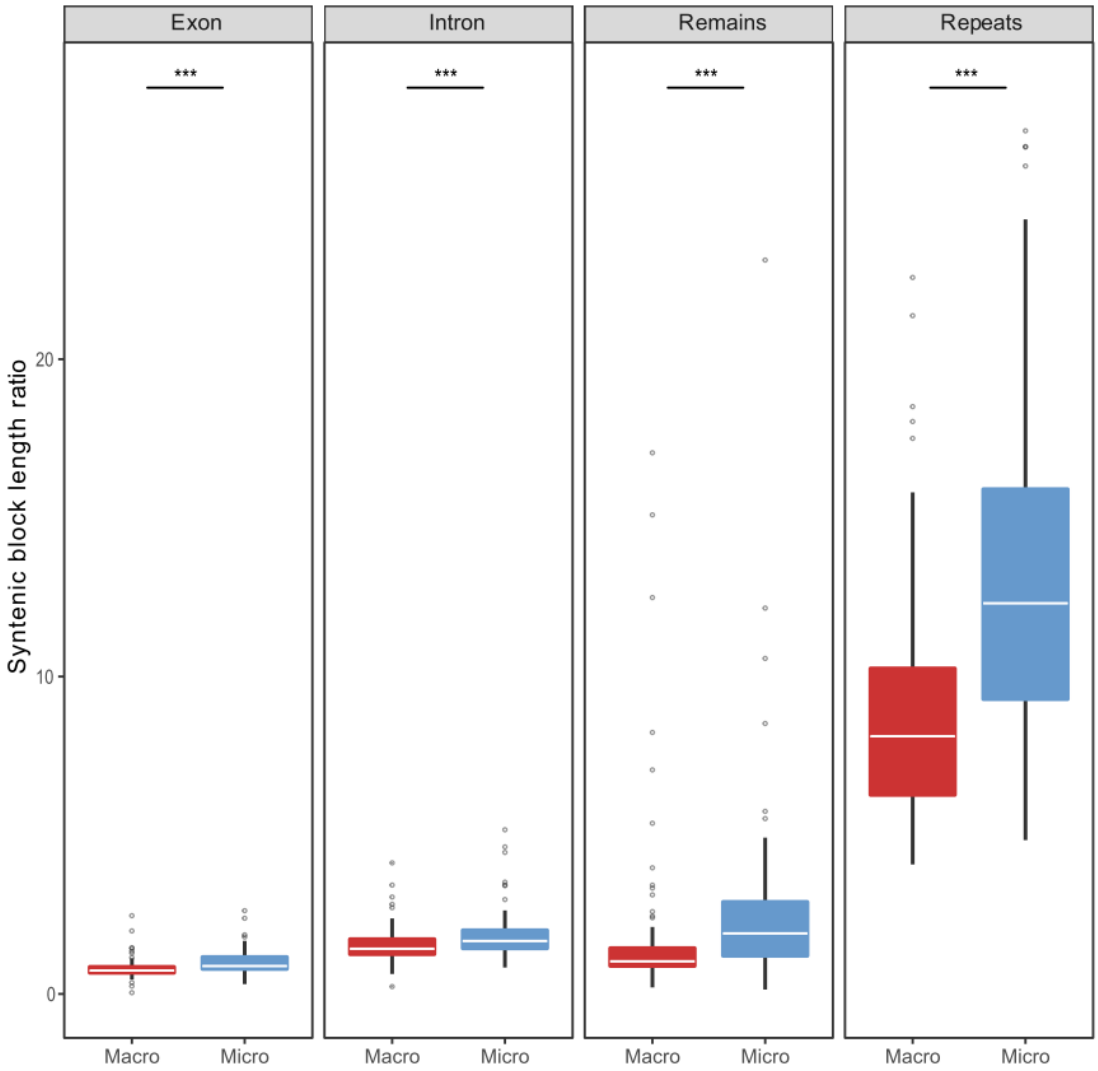

Supplemental Fig. S16. Comparison of length difference between sea turtle and emu in their syntenic blocks across different genomic regions. Microchromosomes show a higher block length ratio for all different types of sequences compared to macrochromosomes. Repetitive regions within the syntenic blocks exhibit a much larger length difference than any other genomic regions, while the exonic regions have maintained around the same lengths. ***: $P < 0.0005$.

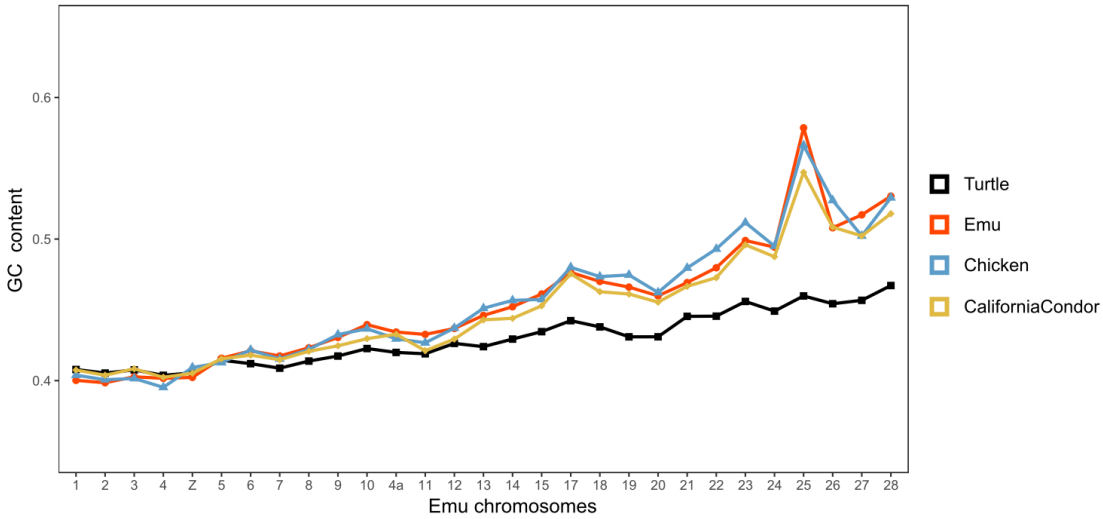

Supplemental Fig. S17. Comparison of GC content on all chromosomes in turtle, emu, chicken and California condor. Microchromosomes in birds tend to have larger GC content when compared to macrochromosomes or to the homologous chromosomes of the green sea turtle.

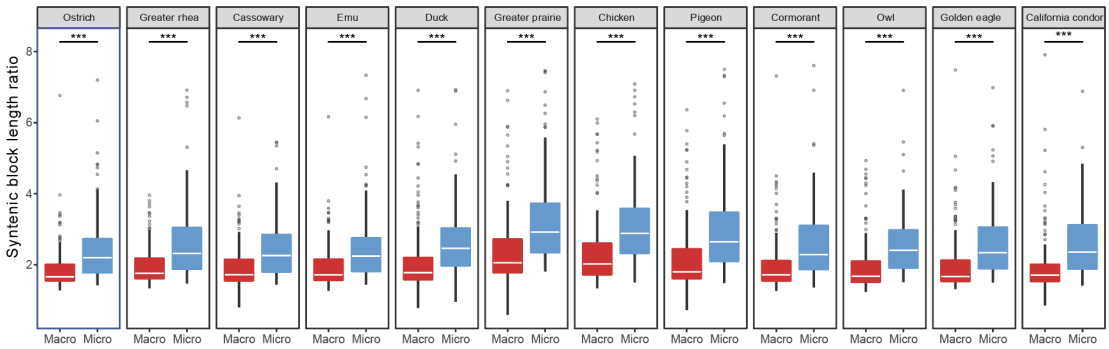

Supplemental Fig. S18. Comparison of length difference between turtle and each bird in their syntenic blocks. Microchromosomes have significantly higher block length ratios compared to macrochromosomes in all investigated species. ***: $P < 0.0005$.

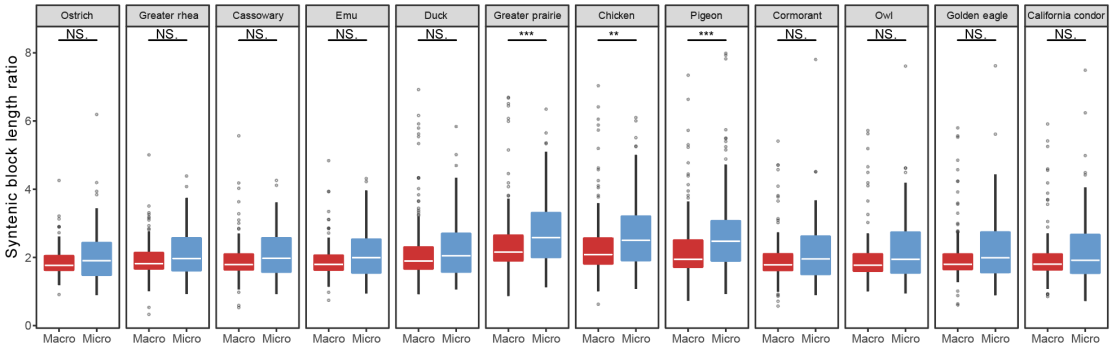

Supplemental Fig. S19. Comparison of length difference between alligator and each bird in their syntenic blocks. Microchromosomes tend to have higher block length ratios compared to macrochromosomes, although the difference in some birds are not significant. **: $P < 0.005$; ***: $P < 0.0005$; NS: not significant.

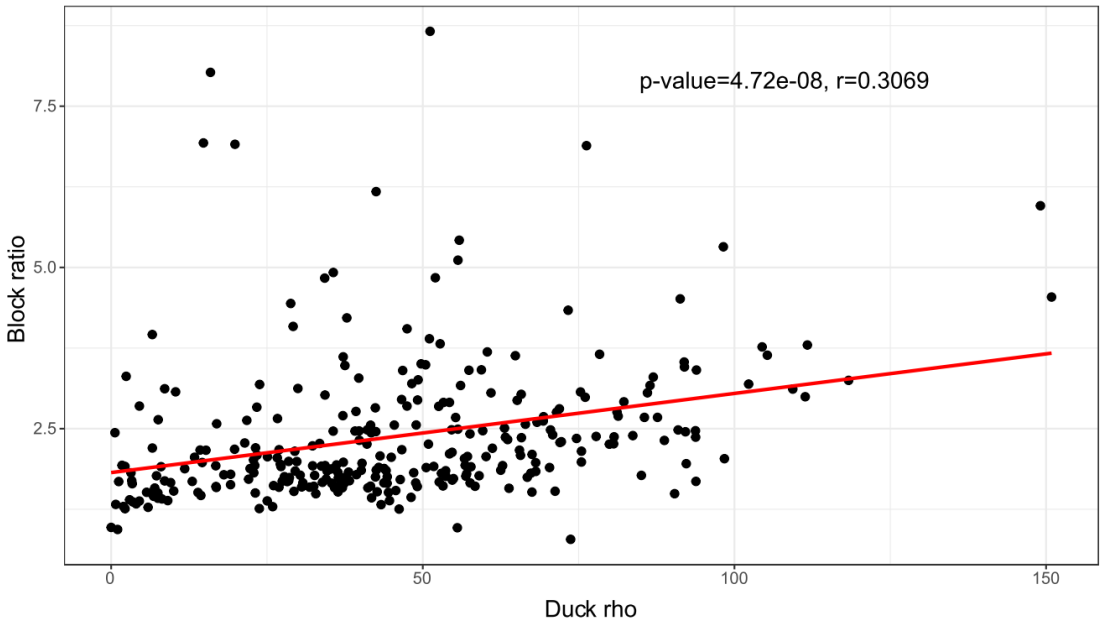

Supplemental Fig. S20. Positive correlation between syntenic block ratio and recombination rate in duck. The recombination rates of duck were derived from the duck study using large genomic resequencing data. Each dot indicates a syntenic block between the green sea turtle and duck.

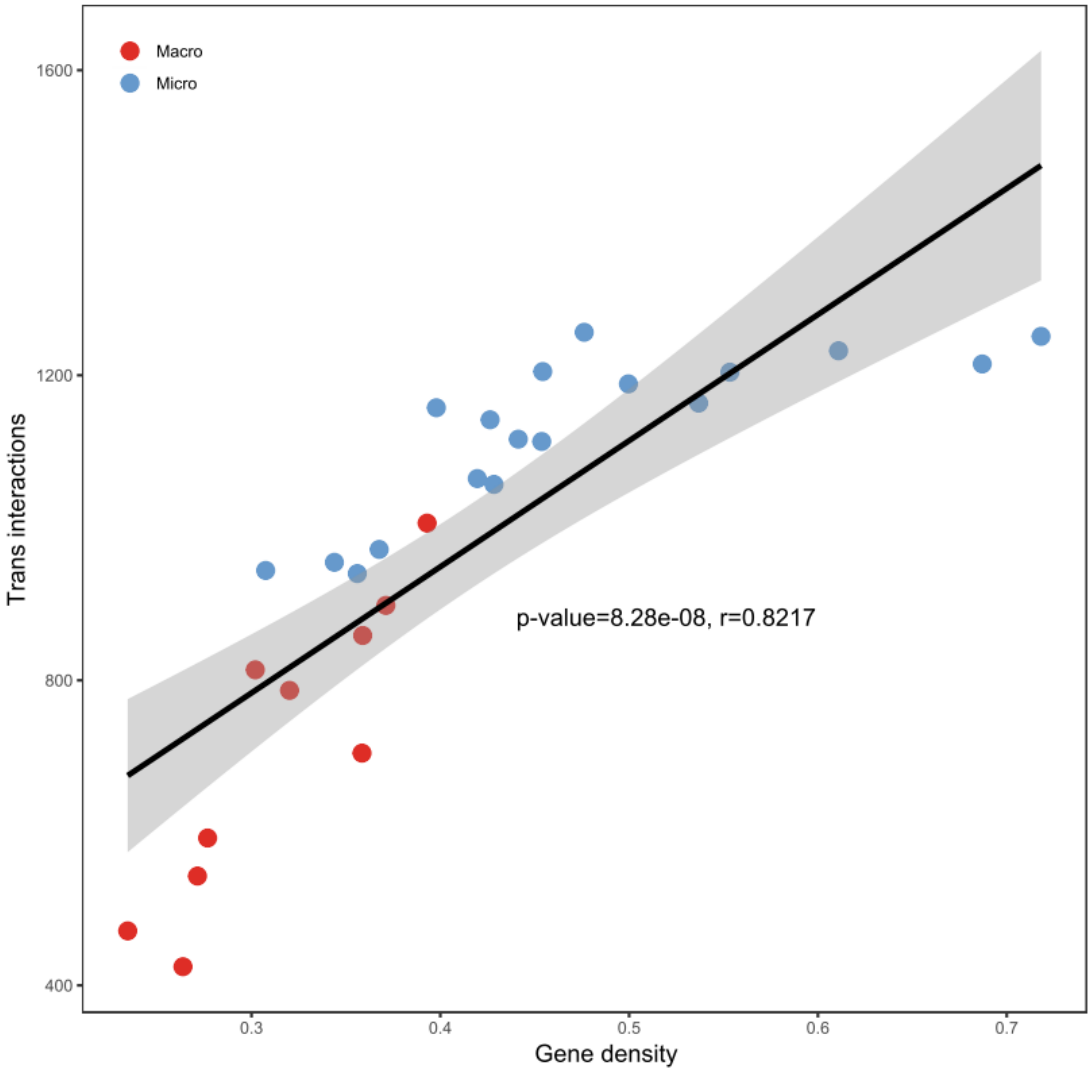

Supplemental Fig. S21. Correlation between gene density and *trans*-interactions across chromosomes. The average gene density and *trans*-contacts were calculated for all emu chromosomes. Gene density significantly correlates with increasing *trans*-interactions from macro- to microchromosomes.

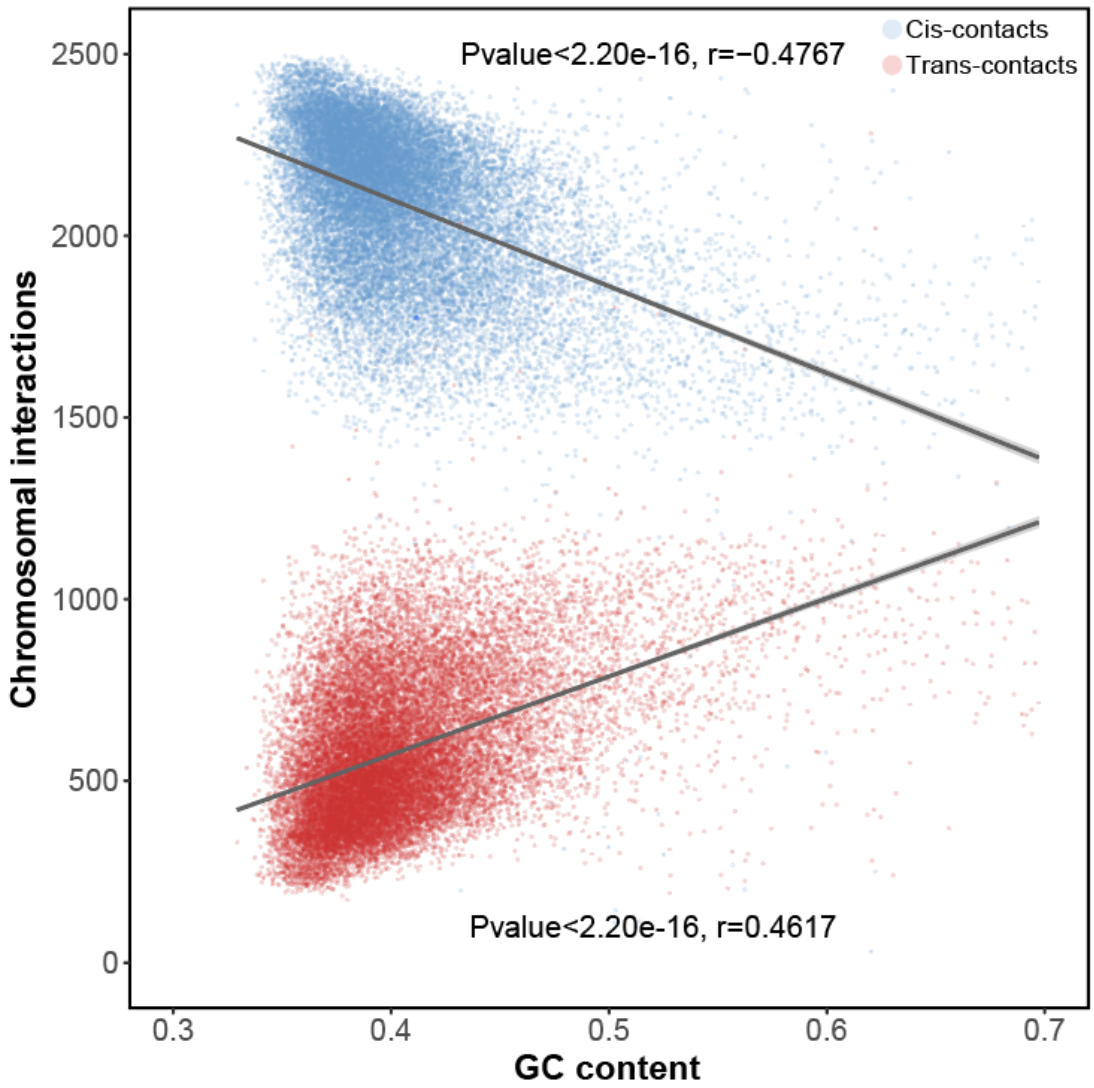

Supplemental Fig. S22. Correlation between GC content and chromosomal interaction on macrochromosomes. GC content and chromosomal interactions were calculated within 40kb non-overlapping sliding windows. Blue and red dots represent the *cis*- and *trans*-contact.

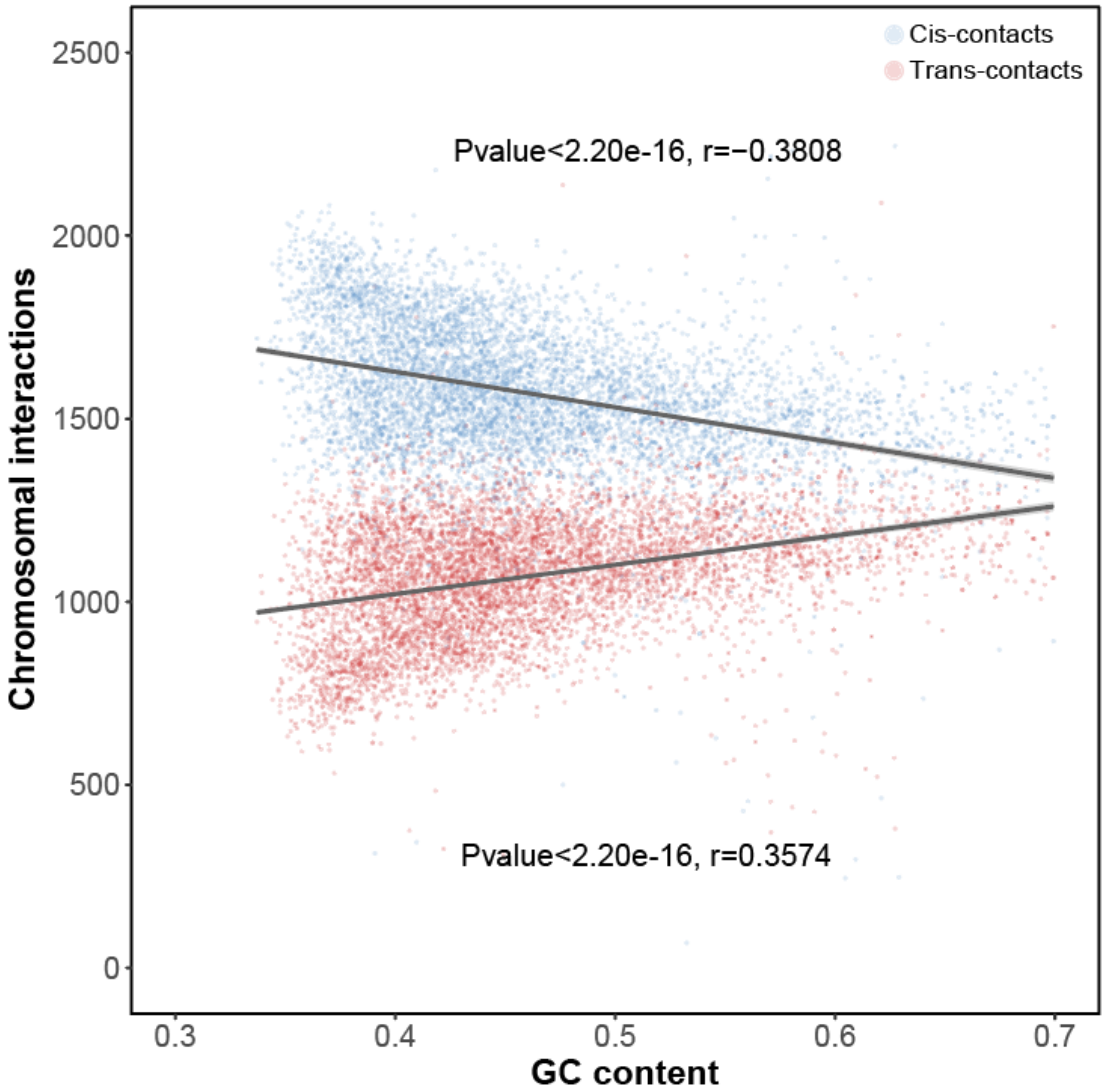

Supplemental Fig. S23. Correlation between GC content and chromosomal interaction on microchromosomes. The legend is the same as **Supplemental Fig. S22**.

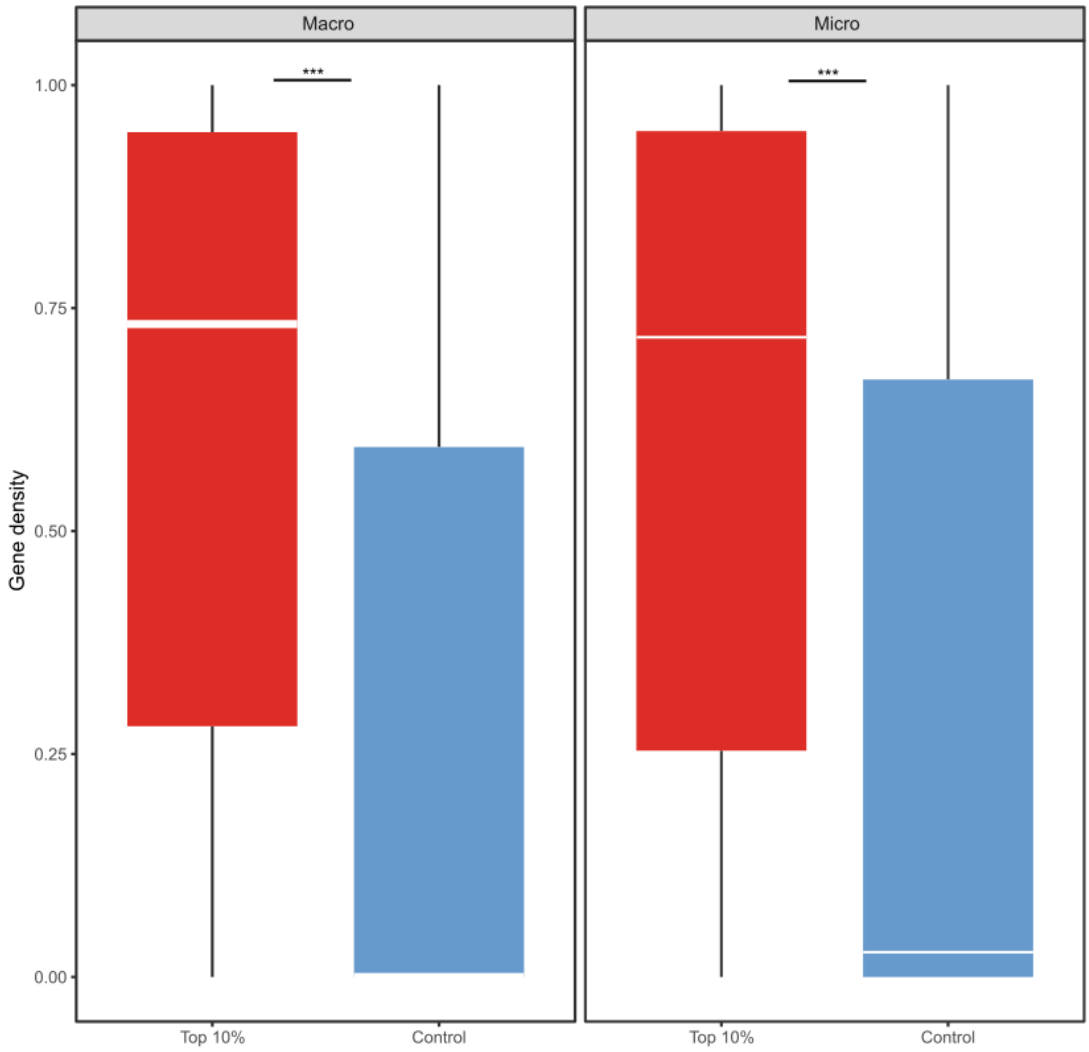

Supplemental Fig. S24. Comparison of gene density between regions with different *trans*-interactions. The regions with robust *trans*-contacts (top 10%) in both macro- and microchromosomes show high gene densities. ***: $P < 0.0005$.

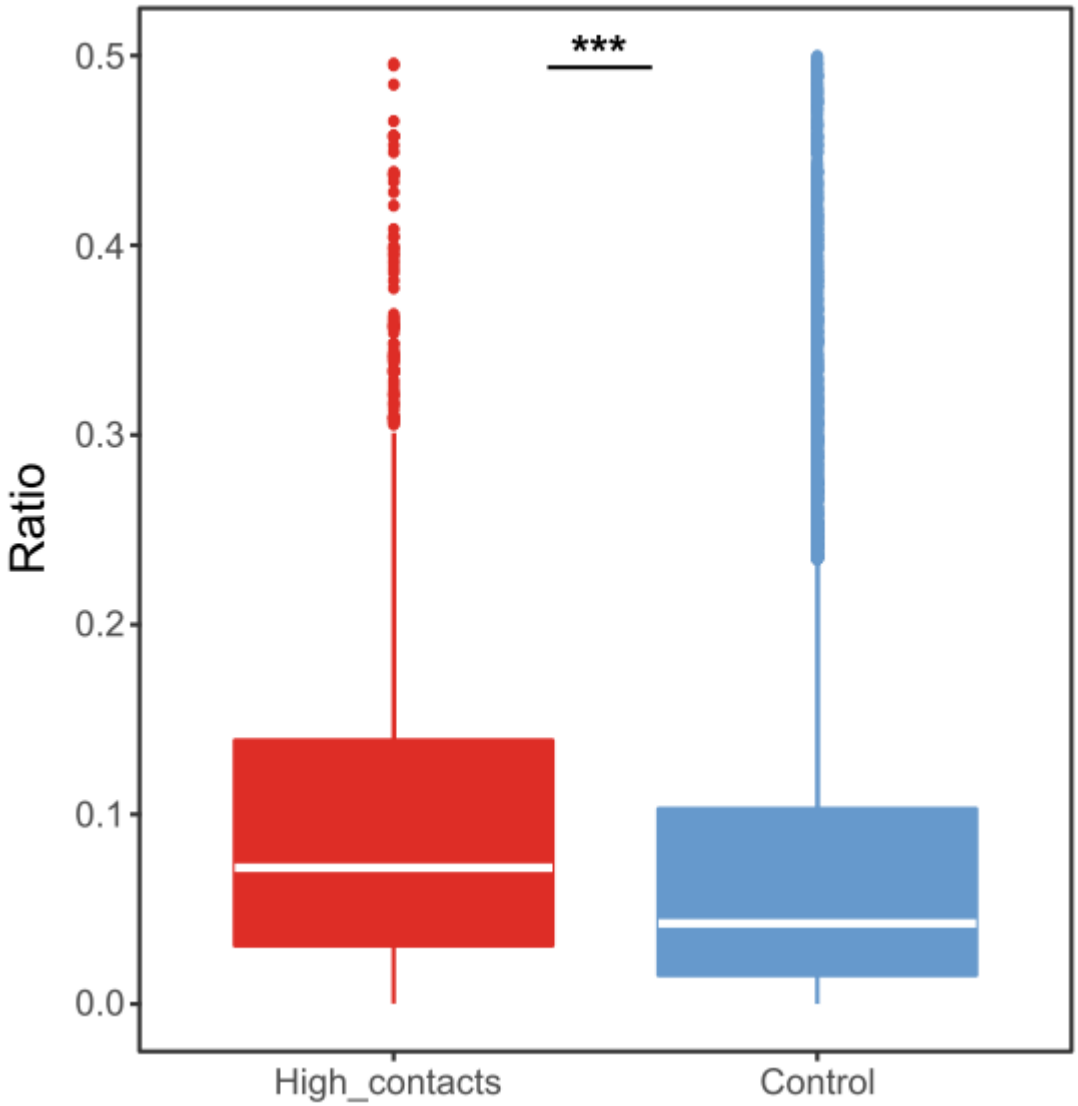

Supplemental Fig. S25. Enrichment for liver-specific genes in the top 10% ranked *trans*-contact regions. The ratio of liver gene expression against the sum of five tissues (liver, brain, kidney, spleen, and ovary) was calculated, as a measurement for the enrichment level of gene expression in the liver. ***: $P < 0.0005$.

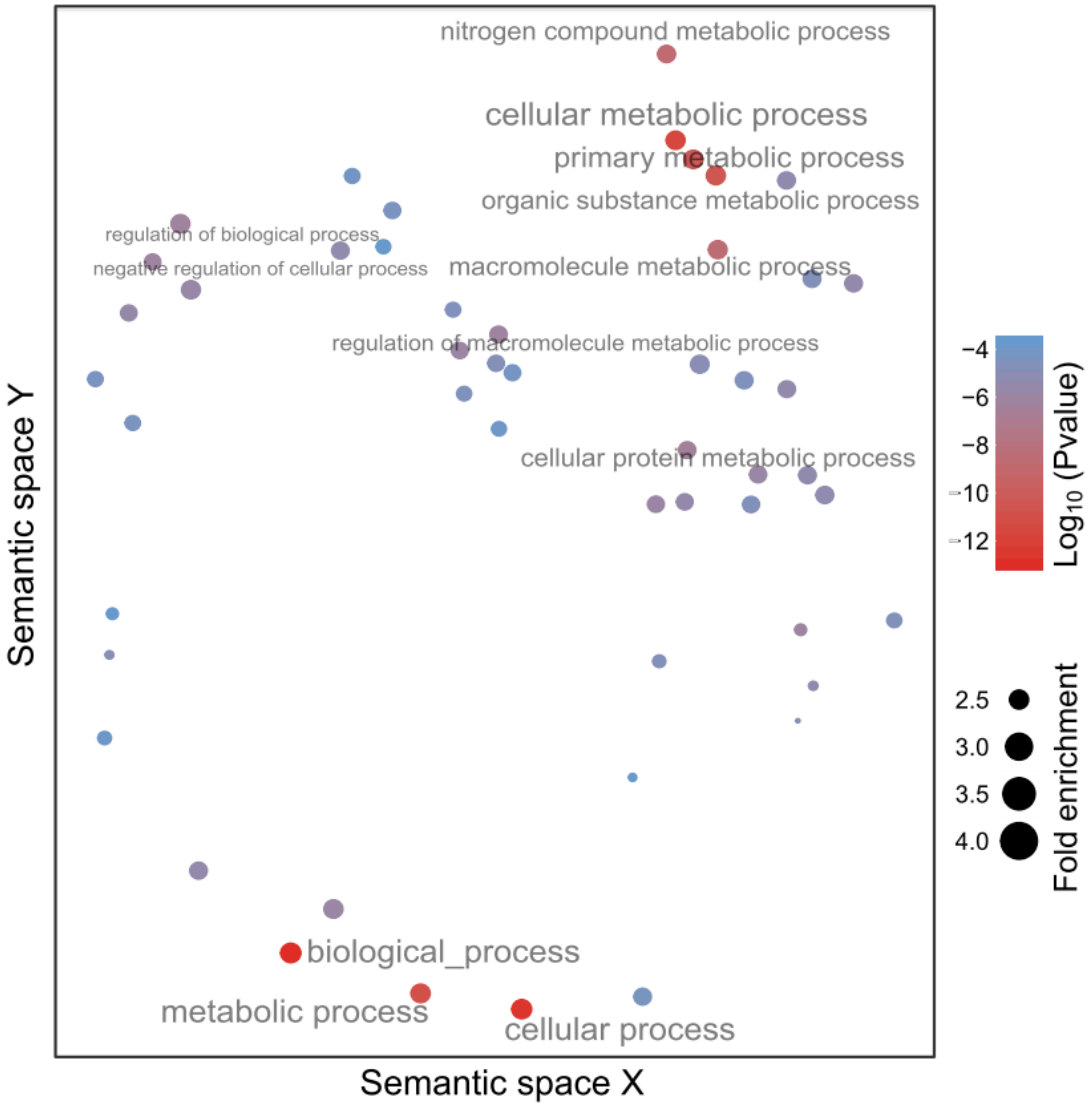

Supplemental Fig. S26. GO enrichment analyses on genes located in high *trans*-interaction regions. We selected genes in the regions with top 10% highest *trans*-interaction and performed GO enrichment analysis using online tools Geneontology (http://geneontology.org/). Revigo was used to draw the plot.

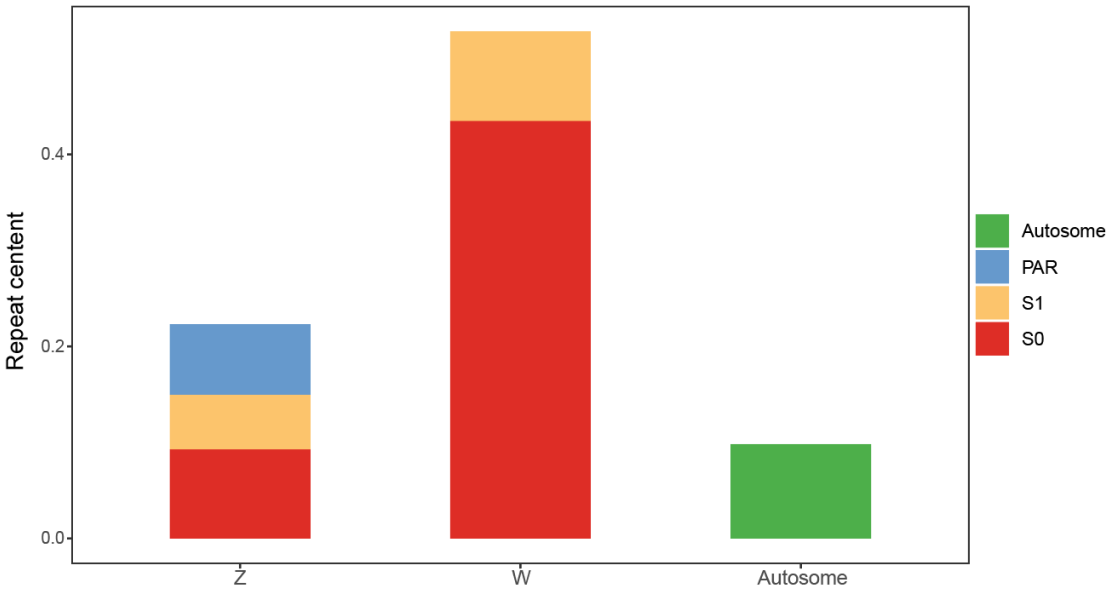

Supplemental Fig. S27. Comparison of repeat content in autosome and ZW chromosomes. The repeat content has dramatically increased in WS0. WS1 has also accumulated more repeats than ZS1.

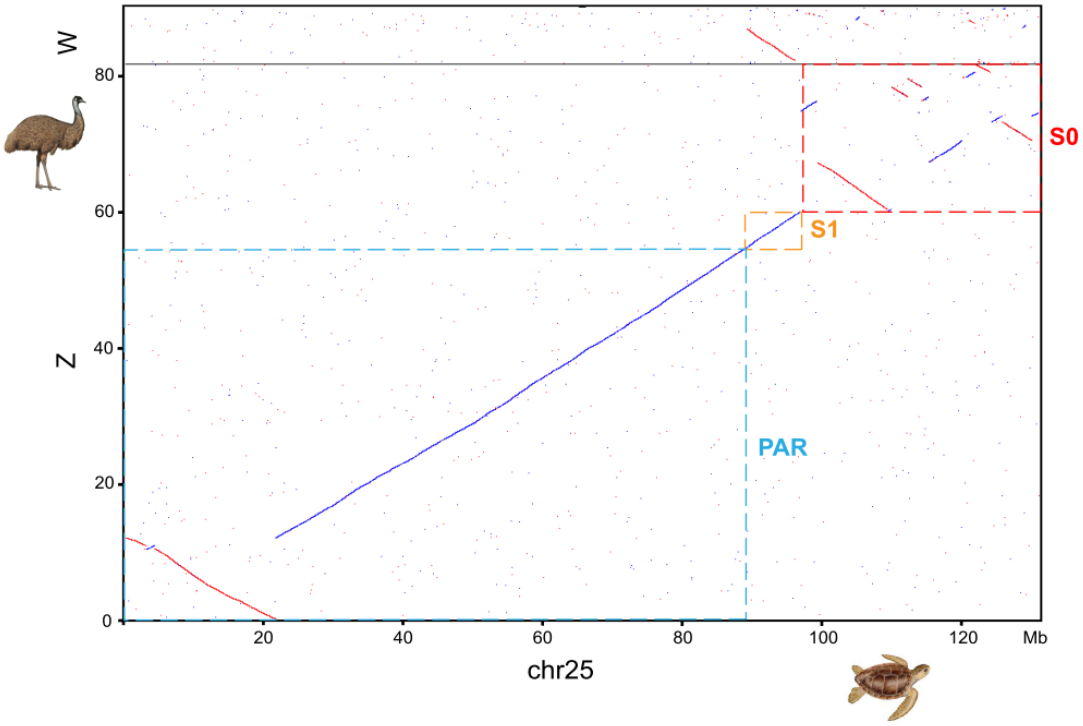

Supplemental Fig. S28. Syntenic dot plot between ZW chromosomes in emu and their homologous autosome in the green sea turtle. The position and name of the PAR and evolutionary strata are indicated by dashed horizontal and vertical lines crossing the dot plot. Emu WS1 formed an inversion compared to the homologous ZS1 and region of turtle Chr25. The emu ZS0 has many more rearrangements than other Z-linked regions.

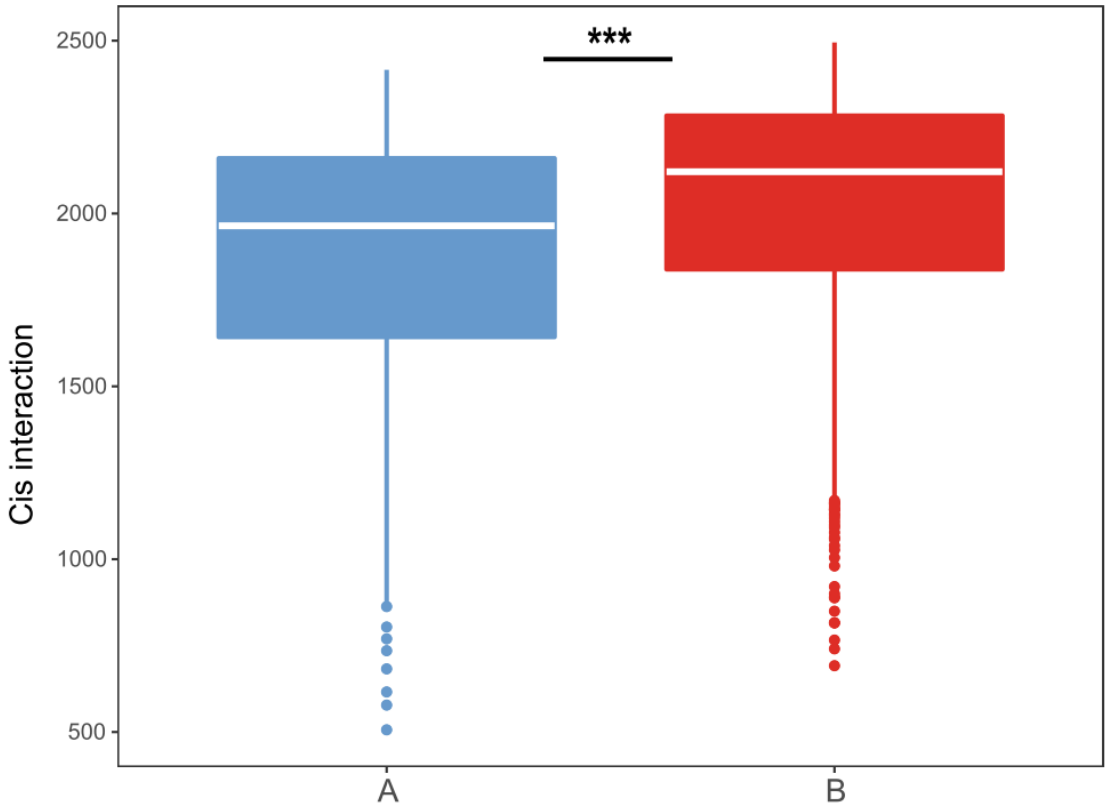

Supplemental Fig. S29. Comparison of *cis*-interactions between active (A) and inactive (B) compartments. The whole genome was divided into A (active) and B (inactive) compartments using the Hi-C 40kb matrix. The interactions of two windows within a same chromosome are *cis*-interaction. ***: $P < 0.0005$.

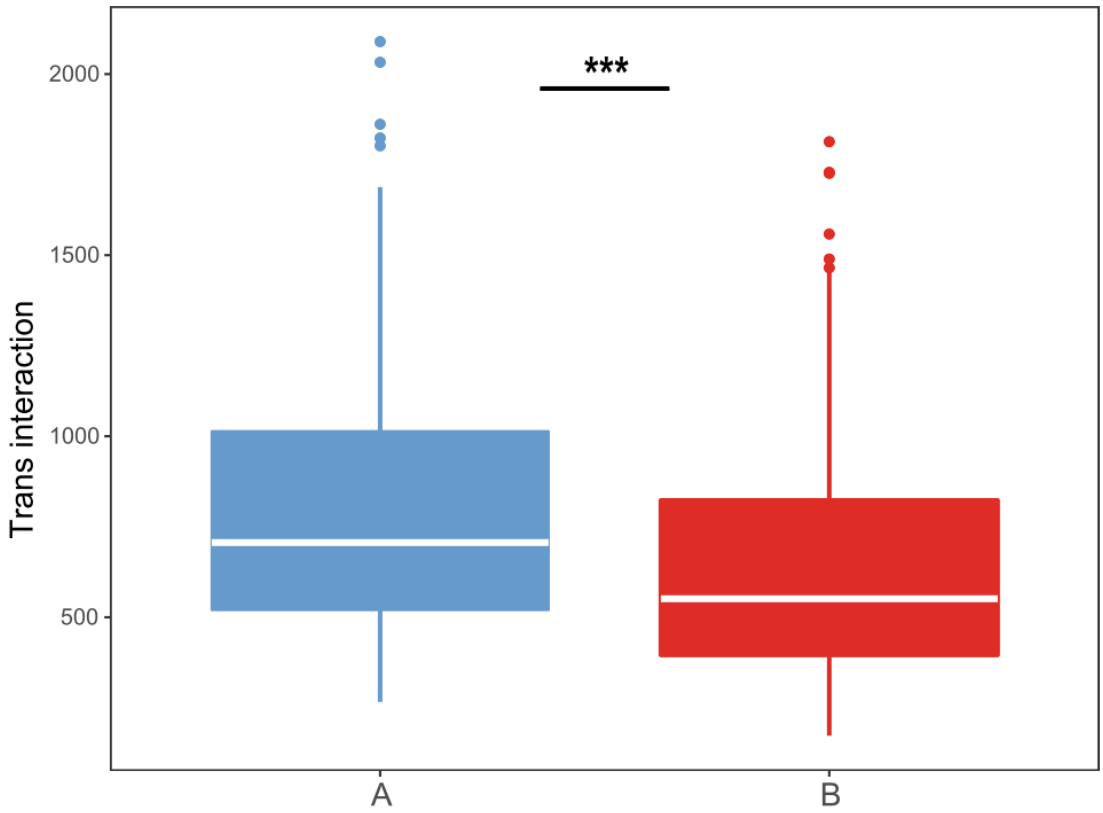

Supplemental Fig. S30. Comparison of *trans*-interactions between active (A) and inactive (B) compartments. The interactions of two windows coming from different chromosomes are *trans*-interaction. ***: $P < 0.0005$.

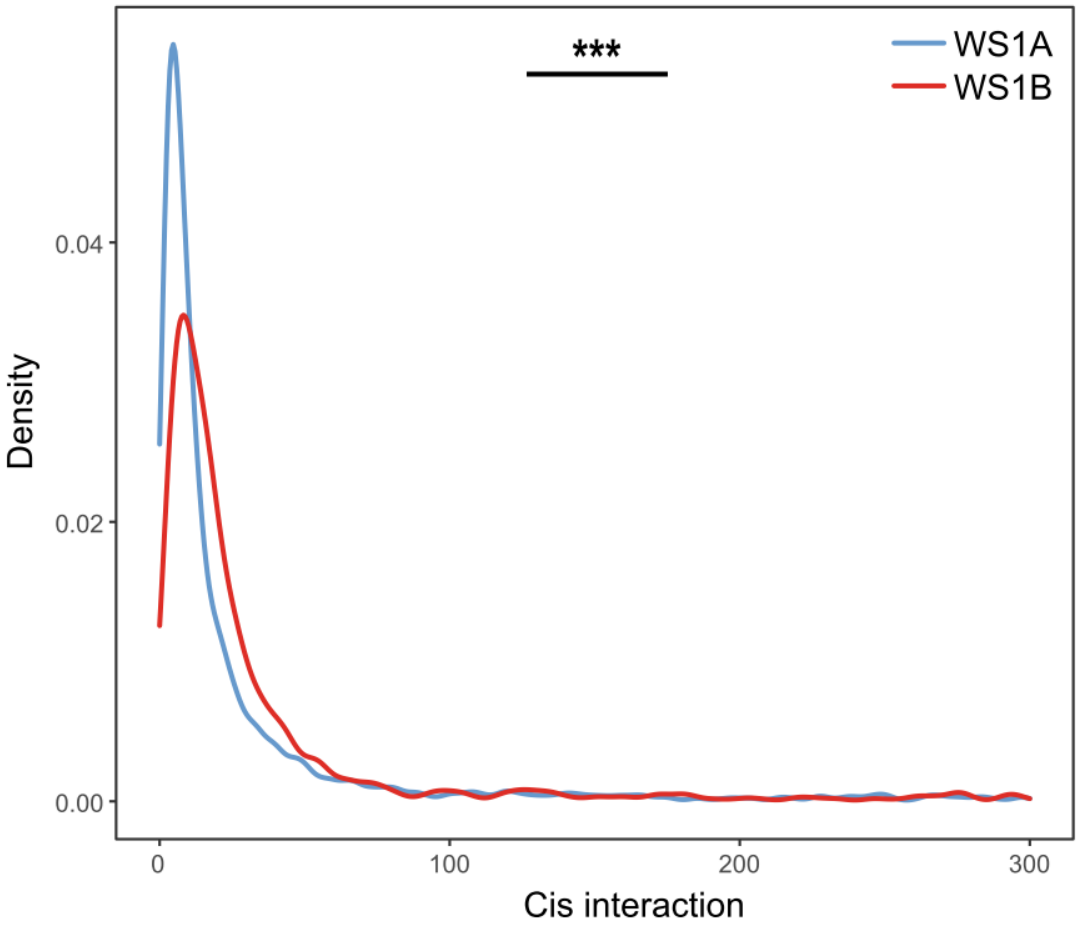

Supplemental Fig. S31. Comparison of *cis*-interactions between WS1B and WS1A. All the interactions of pairwise windows within WS1A and WS1B were used to plot the density plots, separately. ***: $P < 0.0005$.

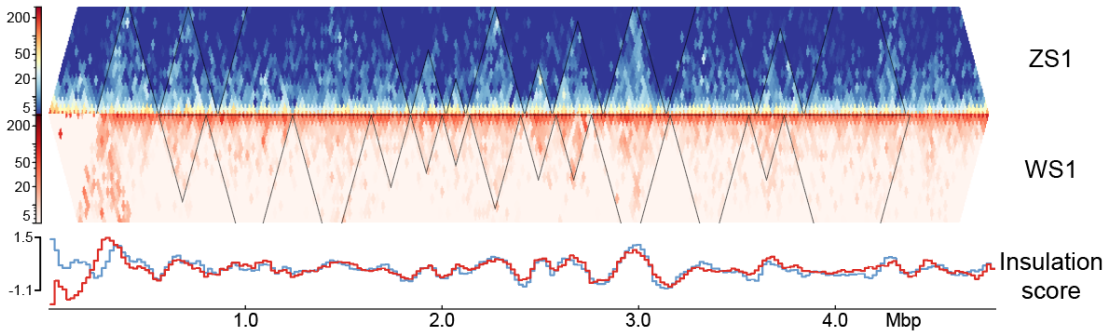

Supplemental Fig. S32. TAD visualization of ZW S1. From top to bottom: TAD of ZS1, TAD of WS1 and TAD insulation score for Z/W, respectively. The black lines indicate TAD domains.